Development of a protocol to obtain the composition of terrigenous detritus in marine sediments -a pilot study from International Ocean Discovery Program Expedition 361

Margit H. Simon[1,2,3*], Daniel P. Babin[3,4], Steven L. Goldstein[3,4], Merry Yue Cai[3], Tanzhuo Liu[3], Xibin Han[5], Anne A. Haws[6], Matthew Johns[3,4], Caroline Lear[7] and Sidney R. Hemming[3,4]

1 NORCE Norwegian Research Centre, Bjerknes Centre for Climate Research , Bergen, Norway

2 SFF Centre for Early Sapiens Behaviour (SapienCE), University of Bergen, Post Box 7805, 5020, Bergen, Norway.

3 Lamont-Doherty Earth Observatory of Columbia University, 61 Rt 9W, Palisades, New York 10964-8000, USA

4 Department of Earth and Environmental Sciences, Columbia University, New York NY, USA

5Key Laboratory of Submarine Geosciences, State Oceanic Administration & Second Institute of Oceanography, Ministry of Natural Resources, Hangzhou 310012, P. R. China

6 Department of Earth and Environmental Sciences, Boston College, Chestnut Hill, MA 02467, USA

7 School of Earth and Ocean Sciences, Cardiff University, UK

 Corresponding author

Highlights
- *application of CsCl-wash leads to significant change in geochemical signature of the sediment*
- *elements in high concentrations in seawater are replaced by Cs+ from the wash*
- *cation exchange wash reveals a truer terrigenous signal*
- *the cation exchange capacity of the sediment may provide additional environmental information*

Abstract

The geochemical and isotopic composition of terrigenous clays from marine sediments can provide important information on the sources and pathways of sediments. International Ocean Discovery Program Expedition 361 drilled sites along the eastern margin of southern Africa that potentially provide archives of rainfall on the continent as well as dispersal in the Agulhas Current. We used standard methods to remove carbonate and ferromanganese oxides and Stokes

settling to isolate the clay fractions. In comparison to most previous studies that aimed to extract the detrital signal from marine sediments, we additionally applied a cation exchange wash using CsCl as a final step in the sample preparation. The motivation behind the extra step, not frequently applied, is to remove ions that are gained on the clay surface due to adsorption of authigenic trace metals in the ocean or during the leaching procedure. Either would alter the composition of the detrital fraction if no cation exchange was applied. Moreover, using CsCl will provide an additional measure of the cation exchange capacity (CEC) of the samples.

However, no study so far has evaluated the potential and the limitations of such a targeted protocol for marine sediments. Here, we explore the effects of removing and replacing adsorbed cations on the clay surfaces with Cs^+, conducting measurements of the chemical compositions, and radiogenic isotopes on a set of eight clay sample pairs. Both sets of samples underwent the same full leaching procedure except that one batch was treated with a final CsCl wash step. In this study, organic matter was not leached because sediments at IODP Site U1478 have relatively low organic content. However, in general, we recommend including that step in the leaching procedure.

As expected, significant portions of elements with high concentrations in seawater were replaced by Cs^+ (2SD 2.8%.) from the wash, including 75% of the sodium and approximately 25% of the calcium, 10% of the magnesium, and 8% of the potassium. Trace metals such as Sr and Nd, whose isotopes are used for provenance studies, are also found to be in lower concentrations in the samples after the exchange wash.

The exchange wash affected the radiogenic isotope compositions of the samples. Neodymium isotope ratios are slightly less radiogenic in all the washed samples. Strontium and Pb isotopes showed significant deviations to either more or less radiogenic values in different samples. The radiogenic isotopes from the CsCl-treated fractions gave more consistent correlations with each other, and we suggest this treatment offers a superior measure of provenance. Although we observed changes in the isotope ratios, the general trend in the data and hence the overall provenance interpretations remained the same. However, the chemical compositions are significantly different. We conclude that a leaching protocol including a cation exchange wash (e.g. CsCl) is useful for revealing the terrestrial fingerprint. CEC could, with further calibration efforts, be useful as a terrestrial chemical weathering proxy.

1. Introduction

IODP Expedition 361, with sites located along Africa's southeastern and southern margin, sought to assess secular variability in Agulhas Current properties and southern African hydroclimates (Fig. 1). To approach documenting changes in either the spatial distribution of rainfall variability or to assess the relationship between sediment sources around southern Africa and Agulhas Current flow, measurement of radiogenic isotope ratios on the clay size fraction of marine sediment was part of the research plan.

Strontium (Sr) and neodymium (Nd) isotopic variations produced by long-lived radioactive decay are well known as powerful tools for the study of provenance of silicate detritus in marine sediment cores. Rb–Sr and Sm-Nd isotopic systems, reflecting the weighted average of detrital components generated in different catchments, provide information on past events of crustal generation and thus represent a powerful means to investigate the provenance of river sediments (Allègre et al., 1996; Goldstein et al., 1984). Sediments derived from older crust have less radiogenic Nd and often more radiogenic Sr isotopes than those derived from younger crust, and a broad inverse relationship between $^{87}Sr/^{86}Sr$ and εNd is thus observed. Prior studies have successfully used the $^{87}Sr/^{86}Sr$ and εNd signatures of lithogenic fractions of terrigenous detritus to infer provenance, transport patterns and continental weathering states on the African continent during the Pleistocene and Holocene (Franzese et al., 2009; Franzese et al., 2006; Hahn et al., 2016; Jung et al., 2004; Rutberg et al., 2005; van der Lubbe et al., 2016). However, none of these studies aiming to target the composition of the detrital fraction have applied a cation exchange wash, which highlights the need for this methodological study. Several processes may make the relationship of the geology in the source area and the ultimate end-members observed at the sedimentary sink difficult to deconvolve, including sediment recycling (e.g. Haughton et al., 1991) differential weathering (Jiménez-Espinosa et al., 2007) sediment sorting by the energy of the transport medium, and diagenetic alteration in the deposited sediments (Morad et al., 2000; Zabel et al., 1999).

Cation exchange washes (e.g. $MgCl_2$) are employed in the preparation of marine sediment to desorb elements from clay surfaces (Gutjahr et al., 2007; Tessier et al., 1979). Gutjahr et al. (2007) employed this method to remove clay-adsorbed ions before leaching the authigenic ferromanganese fraction which was then used for investigating the composition of bottom seawater in the North Atlantic, thus allowing the reconstruction of past water mass signatures (e.g. Gutjahr et al., 2007). For the provenance work that is the goal of this project, both the adsorbed and authigenic fractions need to be removed, and we do not plan to use the dispersed ferromanganese fraction in the sediment fines for water mass proxy measurement. Thus, we decided to perform all of the leach steps as well as the clay separation before the ion exchange washing of the sample. We chose to use CsCl for the cation exchange wash because our goal is to obtain major and trace element chemistry as well as radiogenic isotopes from the clay fraction, and Mg is a major element that we would like to quantify. In contrast, Cs is a very minor element in clays and thus using it as an exchange reagent allows a robust measurement of the Mg concentration of the clays. CsCl is an adequate reagent for the extraction of exchangeable ions as caesium has a large ionic radius but a low charge. This gives it a small hydration sphere, allowing it to form strong bonds with clay surfaces better than any other monovalent or divalent cations. Furthermore, because the Cs exchanged onto the surface will be at levels equivalent to a major element, its abundance in the exchanged clay samples will provide a measure of the concentration of ions displaced from the clay surface, as well as the cation exchange capacity (CEC) of the sample. We reasoned that the CEC of the clays may be related to their weathering history although this is not necessarily a simple relationship.

137 Although this is a minor procedural change, for completeness we decided to
138 determine how the application of a cation exchange wash may impact radiogenic
139 isotopes and other geochemical measurements, as well as clay mineralogy on the
140 same sediment fraction during sample preparation. To our knowledge, this is the
141 first such study to be reported. We selected samples from one of the Expedition 361
142 marine sediment cores in the vicinity of the Limpopo River mouth as this location
143 receives significant detrital input from land.

2. Oceanographic, climatic, and geologic setting

146 IODP Site U1478 is located in the northernmost Natal Valley, on the western flank
147 of Inharrime Terrace (25°49.26′S; 34°46.14′E), ~75 nautical miles east of the
148 Limpopo River (Fig. 1) at a water depth of 488 m below sea level (mbsl). In this
149 study, we show initial results from this recently drilled site, which is sensitive to
150 local river discharge, recovered by IODP Expedition 361 in 2016 (Hall et al., 2017).
151 The Delagoa Bight is a distinct indentation of the continental margin (Lamont et al.,
152 2010) into which the Limpopo River, the second-largest eastward-draining river in
153 Africa, deposits sediment. However, terrigenous material in sediments in that
154 regime can have several potential other source areas including the Incomati, Matola,
155 and Lusutfu river catchments. Surface sediment analysis at a core site very close to
156 Site U1478 demonstrates that the heavy mineral assemblages can be attributed to
157 source rocks in the Limpopo catchment. However, a contribution of Matola and
158 Lusutfu end-members were also detectable (Schüürman et al., 2019).

159 The Delagoa Bight´s hydrography is influenced by the southerly flowing waters from
160 the Mozambique Channel and the East Madagascar Current (Lutjeharms, 2006) the
161 confluence of which forms the Agulhas Current. The Limpopo catchment is a little
162 over 410,000 km^2 and its watershed includes parts of Botswana, Zimbabwe,
163 southern Mozambique and northern South Africa (shaded yellow; Fig. 1). The
164 Limpopo River has a mean annual discharge of ~170 m^3/s and delivers annual
165 sediment loads of 33 Mt/y (Milliman and Meade, 1983). Its system comprises
166 several tributaries with the most significant rivers being the Pienaars; Olifants,
167 Serobaneng, Diep, Upper Mzingwane and Ngez.

168 Under modern climate, the Delagoa Bight´s catchment lies in the transition between
169 tropical and subtropical climate zones, just south of the subtropical ridge between
170 the southern Hadley and the Ferrel cell (Tyson and Preston-Whyte, 2000). Most of
171 the year, surface airflow is from east to west and is stronger during the summer.
172 During winter, the South Indian Ocean anticyclone moves west and the region is
173 under strong subsidence and anticyclonic circulation with very little rainfall. The
174 topographic configuration of the high interior, the escarpment and the coastal
175 lowland and the eastward propagating migratory anticyclones during the synoptic
176 cycle create coastal shallow low-pressure cells associated with Berg winds blowing
177 down the mountains in an offshore direction (Reason and Jury, 1990).

178 The Limpopo River drains the oldest terrane on the African continent. The sediment
179 load (~35 x~ 10^6 ton/yr) is supplied by southern tributaries draining the Kaapvaal
180 Craton (Eglington and Armstrong, 2004) and northern tributaries draining the
181 Zimbabwe Craton (Jelsma and Dirks, 2002) as well as Karoo siliciclastic and basaltic
182 cover. The geology of the highlands is Archean, composed of the Zimbabwe and

183 Kaapvaal Cratons joined by the Limpopo Belt. Bedrock in the cratons, emplaced as
184 early as 3.8 Ga, is characteristically tonalite-trondhjemite-granodiorite, an
185 intermediate, phaneritic, intrusive igneous rock rich in plagioclase and mafic
186 minerals (Kreissig et al., 2000). The Limpopo Belt is a greenstone belt, composed of
187 amphibolite-granulite grade metasediments formed between 2.9 and 2.7 by the
188 collision of the Zimbabwe and Kaapvaal Cratons, the root of a neo-Archean orogenic
189 complex (Kreissig et al., 2000). The isotopic chemical composition of the Limpopo
190 River catchment is distinct in that the highest $^{87}Sr/^{86}Sr$ signatures (between 0.73
191 and 0.80) and most negative εNd ratios (between -26 and -31) are yielded by muds
192 of Limpopo tributaries draining the Kaapvaal and Zimbabwe Cratons. In contrast,
193 Limpopo mud itself has much lower $^{87}Sr/^{86}Sr$, less negative εNd, and a younger
194 (Paleoproterozoic) age than its cratonic tributaries, suggesting more significant
195 contributions from Karoo basalts. Additionally, material from its Pienaars tributary
196 suggests a Paleoproterozoic age, also reflecting contributions from the Karoo
197 Supergroup (Garzanti et al., 2014). We note that Sr isotope ratios are affected by
198 grain size and that the study conducted by Garzanti et al. (2014) used a higher size
199 fraction (<32 μm fraction) than targeted here.

200

201 **3.Methods**
202 **3.1 Sediment leach**

203

204 The detailed laboratory protocol can be found in the research method journal
205 MethodsX. Eight samples were selected from sedimentary depths between 198 and
206 214 m core depth, which approximately, spans the time interval 2.4-2.8 Ma (Hall et
207 al., 2017). In general, the effects of sediment diagenesis under methanogenic
208 conditions in the anoxic zone of the sedimentary column should be considered when
209 sampling to analyse the authigenic phases of marine sediments. This is crucial to
210 consider as, within the methanogenic zone of the sedimentary column, which is
211 anoxic, the originally present authigenic Fe-Mn oxyhydroxides are expected to be at
212 least partially and likely completely removed or altered into other diagenetic
213 mineral phases such as pyrite. Hence the authigenic phases still present in these
214 sediments will have quite different chemical properties and reactivities than
215 sediments in, for example, the sulphate-bearing zone of the sedimentary column.

216 The samples were sieved to separate the >63μm fraction, to save foraminifera for
217 further analyses. The bulk fine sediment (<63μm), (1.7-2.1g material per sample)
218 was decarbonated using 1 M buffered acetic acid solution following the procedure
219 outlined in Gutjahr et al. (2007). This step was repeated 1-3 times until once beyond
220 the application where the sediment no longer appeared to react with the acid.
221 Following carbonate removal the Fe–Mn oxyhydroxide coatings were dissolved by
222 leaching the samples for 24 h, with agitation on a rocker table, at room temperature
223 in a 0.05 M hydroxylamine hydrochloride (HH)–15% distilled acetic acid solution,
224 buffered to pH 4 with analytical grade NaOH. The HH leaching was followed by
225 centrifugation and triple rinses in deionized water. This sequence of procedures
226 deviates from that of Gutjahr et al. (2007) who followed the initial carbonate
227 leaching with a cation exchange step with $MgCl_2$ to desorb cations before leaching
228 the dispersed Fe-Mn oxy-hydroxide for authigenic Nd isotope measurements.

229 Furthermore, we did not use the complexing reagent EDTA as originally suggested
230 in the protocol of Gutjahr et al. (2007) during the leaching of the authigenic Fe-Mn
231 oxyhydroxide fraction.

232 The separation of particles smaller than 2-micron diameter was carried out by
233 settling in a column of water and adding 2mL of 0.5% sodium metaphosphate
234 (calgon) to each tube for the first 2 settling rounds. Particles are assumed to settle
235 in the water according to Stokes Law. For the clay fraction (<2 μm) samples were
236 settled for at least 3 hours and 52 minutes. Settling rounds were performed until the
237 water was clear, usually 15 to 20 iterations. Clods (that is small chunks of clay that
238 are stuck together so the sample can be weighed as a single grain) for the analysis
239 of ^{40}Ar* ages (Gombiner et al., 2016; Hemming et al., 2002) were created after the
240 first settling round by pipetting approximately 300 μg of suspended sediment
241 solution into a micro-centrifuge tube, centrifuging it at high speeds for 30 minutes,
242 and then drying it in the oven at 60°C.

243
244 After the clay separation, a Cs$^+$ cation exchange wash was performed on aliquots of
245 the 8 samples using a 0.1 M CsCl solution. From here forward, this group of samples
246 is referred to as the washed group. After centrifugation and removal of water, 10 mL
247 of ethyl alcohol was added to the sample and vortexed to rinse away excess salt, then
248 the samples were centrifuged, and decanted and the rinsing was repeated a second
249 time. Following the rinsing, samples were dried in an oven at 60°C. Subsamples for
250 measuring ^{40}Ar* were also taken from the aliquot containing CsCl after drying.

251 In this study, organic matter (OM) was not leached because sediments at IODP Site
252 U1478 have relatively low organic content, varying from 0 to 1.25 wt% with an
253 average of 0.45 wt% for the shipboard samples (Hall et al., 2017). However, we
254 acknowledge that even in trace amounts in the clay fraction, OM could significantly
255 impact CEC (pH-dependent). Thus we include a step to leach organic matter in the
256 suggested laboratory protocol. However, it should be considered that in some cases,
257 depending on the sediment properties, an organic oxidative leaching step with
258 hydrogen peroxide (3%) would still not be sufficient to remove various organic
259 phases. Stronger treatments for OM removal can, however, attack the clays and
260 leach away soluble elements including the REE that would affect the trace element
261 measurements. Hence this step might have to be adapted individually according to
262 the setting and sediment composition.

263
264 **3.2 Sediment dissolution**
265
266 About 20 mg samples of homogenized and powdered material from the clay fraction
267 were weighed and completely dissolved using a mixture of concentrated HF-HNO$_3$-
268 HClO$_4$.

269 The dissolution of the sediment was conducted by pipetting 500μl concentrated
270 nitric acid (double-distilled 16N HNO$_3$) into the sample beaker and sonicating for
271 ~20 minutes to 1 hour to disaggregate the material. Thereafter 200μl of perchloric
272 acid (optima grade) was added to the sample to remove organic matter and renewed
273 sonication of the solution in the beakers was performed. Afterward, 600 μl of

concentrated HF (optima grade) was pipetted into the sample and the beakers were heated on a hot plate at 150°C overnight (>12 hours). After 12 hours, the solution should be completely clear and have no suspended solids. In some cases, the sample had a black ring around the edge of the beaker likely resulting from undigested organic matter. These samples required the addition of further perchloric acid and heating. We performed a first evaporation step by heating the beakers uncapped on the hot plate at 200°C. Thereafter 1 mL of 8N HNO_3 was added to the beaker to perform the second dissolution step. Samples were heated in capped beakers at 150°C on the hot plate for 2 or more hours to ensure full dissolution. Thereafter beakers were uncapped to perform the second evaporation and heated at 175-200°C. The final dissolution of the samples was performed by adding 1mL 4N HNO_3 and heating the solution at 150°C and occasional sonification until samples have gone into full solution.

Sediment standard from the Japanese Geologic Survey, JLk-1 (Japanese lake sediment) was dissolved alongside the 16 unknown aliquots used in this study (Imai et al. (1996).

3.3 Major/trace element analysis

Major and trace element analyses were carried out using an Agilent Technologies quadrupole ICP-MS at the Facility for Isotope Research and Student Training at Stony Brook University. The 16 samples were measured alongside sediment standard JLk. Major and trace elements were measured simultaneously from solutions with 20,000 dilution. A mixture of all of the diluted samples was concocted as a drift solution to monitor and correct for instrumental drift. The pattern of measurements was blank, drift solution, unknown, unknown. Standards were measured with the pattern blank, drift solution, standard, twice each at the beginning, middle, and end of the analytical sessions. Samples were replicated over two sessions that took place within 24 hours. The drift solution was also used to correct the offset between runs. Signal intensities were converted using the signal intensity from 12 measurements on JLk and the concentrations from Imai et al. (1996). Precision is estimated by comparing sample replicates. For precision, we report the sample averaged percent standard deviation for each element (2SD). Precision for the major elements except Ca is better than 2%. The precision for trace elements reported here is better than 4%. Due to high Ca background and low sample Ca abundance, precision for that element is 12%. For one run, Ca had to be discarded. To achieve an accurate measurement of Cs, we applied the standard addition technique. We added 40 μl of a 100 ppm Cs solution (4 μg of Cs) to an aliquot of each Cs washed sample. To determine sensitivity to Cs, this was measured alongside an unspiked aliquot of that sample.

Concentrations of Cs determined using standard addition were converted to cation exchange capacities using the equation:

318
$$CEC = \frac{[Cs]}{\frac{M_{Cs}}{Q_{Cs}} * 10}$$

319

320 Where [Cs] is the concentration of Cs in a sample, in ppm. M_{Cs}/Q_{Cs} represents the
321 equivalent weight of a Cs atom, where M_{Cs} is the molar mass of Cs, and Q_{Cs} is the
322 valence of Cs (+1). The 10 is a conversion factor to convert equivalent weight,
323 usually reported in grams/equivalent, to 100g/milliequivalent (meq). Using this
324 equation will result in units of meq/100g, a common unit for reporting cation
325 exchange capacity.

326
327 **3.4 Radiogenic isotope analysis**
328

329 The Sr, Nd, and Pb isotopic measurements were performed at the Lamont-Doherty
330 Earth Observatory (New York) using a ThermoScientific Neptune Plus multi-
331 collector ICP-MS in static mode. Pb was extracted using Bio-rad AG®1-X8 resin and
332 HBr and HCl column chromatography. Nd was extracted using Tru-Spec® resin
333 followed by Eichrom Ln-Spec® resin and HNO_3. Sr was extracted using Eichrom Sr-
334 Spec® resin. The total procedural blanks for Pb in hotplate digestions range from
335 21-30 pg and the blanks for Nd and Sr are negligible. The MC-ICP-MS instrumental
336 drift is monitored by standard-sample bracketing using JNdi-1 for Nd, NBS 987 for
337 Sr, and NBS 981 for Pb. Typically 30–70 standards and 20–30 samples are analysed
338 during a session and reported 2SD external errors are estimated from the
339 reproducibility of the standards. These are 0.2 for ε_{Nd} and 0.000019 for $^{87}Sr/^{86}Sr$.
340 For $^{206}Pb/^{204}Pb$ we report a standard reproducibility error of 0.001795; 0.0024297
341 for $^{207}Pb/^{204}Pb$ and 0.007317 for $^{208}Pb/^{204}Pb$. We collected 60 ratios for each run
342 using 200 ppb solutions for Sr and Pb and 100 ppb solutions for Nd. Reported values
343 are corrected to those of the international standards. Samples were corrected to the
344 accepted value of the JNdi-1 standard of 0.512115 (Tanaka et al., 2000) for
345 $^{143}Nd/^{144}Nd$, NBS 987 standard of 0.710248 for $^{87}Sr/^{86}Sr$ (Weis et al., 2006), and
346 NBS 981 for 16.9405 for $^{206}Pb/^{204}Pb$; 15.4963 for $^{207}Pb/^{204}Pb$ and 36.7219 for
347 $^{208}Pb/^{204}Pb$ (Abouchami and Galer, 1998). In-run mass fractionations was corrected
348 using $^{146}Nd/^{144}Nd = 0.7219$ and $^{86}Sr/^{88}Sr = 0.1194$ Pb isotopes were doped with Tl
349 in a proportion of Pb/Tl = 5. In-run mass fractionations were corrected
350 using $^{205}Tl/^{203}Tl$ value of 2.388. Quality control was provided by measurements of
351 rock standards BCR-2 and JLK for Pb, BCR-2, JLK and BHVO-2 for Sr, BCR-2, JLK and
352 BHVO-2 for Nd, all of which were repeatedly run through the entire dissolution and
353 chemical separation procedures (Supplementary Table 4). The $^{143}Nd/^{144}Nd$ ratios of
354 the samples are reported as ε_{Nd}, which is the parts per 10,000 deviation of the
355 $^{143}Nd/^{144}Nd$ value from the present-day Chondritic Uniform Reservoir (CHUR) value
356 of 0.512638 (Jacobsen and Wasserburg, 1980).

357
358 **3.5 K/Ar age analysis**
359

360 Aliquots of the clay fraction were removed from the <2 μm fraction of both washed
361 and unwashed samples and dried in 1 mL micro-centrifuge tubes after the settling

process. Samples were removed from micro-centrifuge tubes, weighed, and loaded into a 32-spot copper disk - typically in pairs of duplicates for 14 samples - plus 4 GLO-1 glauconite standard (Odin, 1976). To obtain a reproducible age for a sample, we found it important to weigh and load the entire clod. Sample weights in this study ranged between 0.1 and 0.5 mg.

For each measurement session, the pattern of runs includes blanks at the beginning and end of the session bracketing the entire sequence of runs. Each air standard was bracketed by a blank measurement, and each set of 3 unknowns or GLO-1 measurements is bracketed by a blank/air/blank sequence. Signal intensities of the airs, unknowns, and GLO-1 are well above the background levels, and blank corrections are estimated from the most recently measured preceding blank. Air standards are used for quality control, to correct for any instrument drift, and to estimate the correction for the atmospheric component in the samples to yield the ^{40}Ar* (that is the radiogenic argon from the decay of K in the sample). GLO-1 standards are used to quantify the sensitivity of the instrument during the session. GLO-1 has 1.109e^{-12} moles of ^{40}Ar* per mg of sample (Odin, 1976). The sensitivity of the mass spectrometer/extraction line system for argon is ~5.13e^{13} nannoamps/mole. Signals are measured on an analogue multiplier with high voltage set such that 1 nannoamp is approximately 10 mv on a 10^{11} Ω resistor. The reproducibility of the age of GLO-1 is between 1 and 2 % for most sessions (2 SD). Reproducibility of the sediment clods is not generally as good as for the GLO-1, and when the difference between aliquots is >10%, additional aliquots of the sample are repeated in another session.

3.6 Clay mineral analyses

Clay mineralogy determinations were performed under three conditions, *i.e.*, air-drying, ethylene-glycol solvation for 24 h, and heating at 490 °C for 2.5 hours, by standard X-ray diffraction (XRD) on a PANalytical X'Pert Pro diffractometer in Key Laboratory of Submarine Geosciences, China, SOA with CuKα radiation and Nifilter, under a voltage of 45 kV and an intensity of 40 mA. Identification of clay minerals and calculation of their relative proportions were made according to the position and area of the (001) series of basal reflections on the three XRD diagrams (not shown), *i.e.,* smectite (001) including illite/smectite mixed-layers at 17Å, illite (001) at 10 Å, and kaolinite (001) and chlorite (002) at 7 Å (Biscaye, 1965). Relative proportions of kaolinite and chlorite were determined based on the ratio from the 3.57/3.54 Å peak areas. Additionally, illite crystallinity was obtained from the full width at half maximum (FWHM) of the 10 Å peak (Esquevin, 1969). Semi-quantitative calculations of all the included peak parameters were performed on the glycolated curves using Jade6. Clay mineral analyses were performed on oriented mounts. Results on the washed fraction can be found in the supplementary information.

4. Results

4.1 The effects of adsorbed cation removal and CsCl wash on clay geochemistry

4.1.1 Major and Trace Elements

Here we assess which elements were exchanged during the procedure as well as the effectiveness of the exchange wash. Figure 2A depicts how the wash changes the composition of the samples via cation exchange. The differences in concentrations, including uncertainties, between washed and unwashed aliquots are shown. Note the log scale, used to accentuate changes in concentration. All of the data reported here are from samples dissolved with HF, so Si was lost. Most notable here is that by far and away, Cs is replacing Na on the clay surfaces. Sodium concentration is reduced by 75% on average. Less outstanding is the loss of other soluble major elements: Ca (22%), Mn (14%), Mg, (14 %), and K (8%). Ca concentrations in the clay are extremely low (~0.12 g/100g), and tuning the quadrupole mass spectrometer to achieve precise measurements on this low abundance major element, the other major elements, and trace elements simultaneously was a challenge. Concentrations of elements predominantly integrated into the structure of clay minerals, such as Al, Fe, and Ti, are not changed by the wash outside of the reported analytical uncertainty. Concentrations of trace metals Sr and Nd, used by geochemists as isotopic tracers, appear to decrease as a result of the exchange wash by 25%.

We test the effectiveness and quality of the exchange using a charge balance. However, this balance is not trivial because mass is not conserved in the exchange reaction. Replacing light elements like sodium with the heavier element caesium creates an appreciable weight difference between the washed and unwashed samples. So first we simulate a "mass balance" by estimating what percent of each major element is lost, on average. We determine what fraction that element contributed to the total losses by summing those percents and normalizing them to 100. For example, about 75% of Na is lost in each sample during the washing, but this represents only ~60% of total ions exchanged. To simulate this "mass balance," we model the weight change of replacing each element (e.g. Na, 23g/mol) with Cs (133 g/mol) at the percent it contributed to the cations exchanged. The above calculations reveal each sample is ~5g/100g heavier after the exchange wash. The calculation process artificially removed this extra weight.

To complete the charge balance, we take exchangeable major element oxides (Na, Mg, K, Ca, and Mn) and convert them first to moles, and then to equivalents using their atomic charge. Ideally, the charge of the exchangeable cations lost and the charge of Cs^+ ions gained should sum to zero. Therefore, we visualize the charge balance as a cumulative sum (Fig. 2B). The bulk of the charge displacement comes from Na and Mg, as noticed previously. Of the 8 samples, 4 return to zero within error. 3 samples gained more Cs than they lost exchangeable cations. One sample does not appear to have gained enough Cs. See the discussion section for potential explanations for this apparent charge imbalance. We admit that these results are troubling, as they would cause us to question the accuracy of our Cation Exchange Capacity measurements. We believe this is a function of accumulated uncertainties, but more tests should be performed to increase the confidence in the CEC.

4.1.2 Radiogenic Isotopes

Six of 8 washed samples have $^{87}Sr/^{86}Sr$ values that are significantly lower (beyond measurement error) than their non-treated counterparts (Fig. 3A, Supplementary Table 1). Washed samples have uniformly less radiogenic εNd values (Fig. 3B), beyond the measurement error (Supplementary Table 1). Pb isotopes are not uniformly affected by the cation exchange wash. Four out of 8 samples have more radiogenic Pb isotopic ratios, and four out of 8 have less radiogenic Pb isotopic ratios (Fig. 3F-J). They correlate strongly with each other ($R^2 = 0.80$-0.97), but less strongly to other measures of provenance (εNd: $R^2 = 0.3$-0.63, $^{87}Sr/^{86}Sr$: $R^2 = 0.29$-0.36, and Ar: $R^2 = 0.034$-0.34)(not pictured).

$^{40}K/^{40}Ar$ ages from the washed samples are systematically younger than from the unwashed aliquot (Fig. 3C) and they have lower %radiogenic ^{40}Ar. Of 8 sets of samples, 7 unwashed samples are 4-10% older than their washed counterparts. Two unwashed sample, MS22 and MS 34 yielded ages which are 15 -22 % older, respectively. The unwashed samples, in general, are less reproducible (Fig. 3C), and subsequently we found that because of this small-scale heterogeneity it is necessary to weigh the entire clod to get consistent results.

There are many reasons why different isotope systems used as provenance indicators may yield different results from each other, such as the varying temperatures at which different systems close and how they are affected by diagenesis, weathering, and clay mineral formation. However, in principle, we would expect that they show some similarities, reflecting the chemistry of their source regions. Therefore, we compare trends in isotope systems and quantify these using linear regressions. We argue that if the correlation changes, it is most likely the result of authigenic phases biasing the radiogenic isotope signature.

We present a linear regression of each isotope ratio used for provenance to all the others for both the unwashed (Fig. 4A-F, left panel) and the washed group (Fig. 4A-F, right panel). The application of our procedure resulted in trends in isotopic compositions within the washed group that more resemble each other: the regressions from the washed group have higher correlation coefficients. These data demonstrate how the wash affected the composition of radiogenic Sr in our samples. Before the wash, εNd does not have a strong correlation with $^{87}Sr/^{86}Sr$ ($R^2 = 0.25$) (Fig. 4A). There is weak correlation between the ^{40}Ar model age and $^{40}K/^{40}Ar$ with $^{87}Sr/^{86}Sr$ ($R^2 = 0.2$, 0.04)(Fig. 4B-C). When radiogenic isotope measurements are compared amongst the washed group, the trends between each isotope system are more obviously systematic. The relationship of $^{87}Sr/^{86}Sr$ to εNd and $^{40}K/^{40}Ar$ is most improved with an R^2 improving from 0.25 to 0.6 and from 0.05 to 0.49 respectively (Fig. 4A; C).

As expected, the ^{40}Ar model age, calculated assuming a uniform 2% K, correlates strongly with the $^{40}K/^{40}Ar$ age, which is calculated with the measured K ($R^2 = 0.87$). The $^{40}K/^{40}Ar$ age correlates more strongly with εNd than the ^{40}Ar model age (Fig. 4D, E), ($R^2 = 0.62$ vs $R^2 = 0.56$). The relationships of all of these isotopic tracer proxies are improved by the wash, but less dramatically than for Sr isotope composition.

Matrices of correlation coefficients were generated to evaluate the effects of the procedure. Fig. 4G shows the R^2 coefficients before the procedure, amongst the unwashed group, and Fig. 4H shows the R^2 coefficients after. The effects of the procedure are best visualized by subtracting the before (Fig. 4G) and after (Fig. 4H) matrices to generate a matrix of anomalies (Fig. 4I). Correlations of $^{87}Sr/^{86}Sr$ to $^{40}K/^{40}Ar$ and εNd are notably improved by the CsCl wash, with the highest anomaly and warmest colors (Fig 4I).

4.2 Clay mineralogy

The major clay minerals in the samples were identified by X-ray diffraction techniques (Fig. 5). In general we find that illite is the most abundant, smectite is second, and kaolinite is third. Chlorite could not be detected in the 8 samples. Illite values range from 29 to 50 % in the unwashed fraction and tend to increase down-core. Smectite has a range of values from 24 to 42% and showing a decreasing trend over time. Kaolinite seems to vary around a mean between 21-30% (Fig. 5). Further details on the clay minerals in the washed aliquot can be found in the SI.

4.3 Chemical Index of Alteration (CIA) and Cation exchange capacity (CEC) of the clay fractions

The Chemical Index of Alteration (CIA), (Fig. 3D) estimates the extent of weathering of continental rocks and sediments, where higher values indicate greater alteration, and is very useful in the interpretation of marine sediments (Nesbitt and Young, 1982b).

$$CIA = 100 * Al_2O_3/(Al_2O_3 + CaO + Na_2O + K_2O)$$

Cation exchange capacity (CEC) is used in agriculture as an assessment of soil fertility, indicating the capacity of the soil to retain several nutrients (e.g. K^+, NH_4^+, Ca^{2+}) in plant-available form. The extent of weathering of soil can be estimated from its CEC, as the availability of exchangeable cations depends on clay mineralogy, which is a function of the substrate composition and degree of chemical weathering.

We calculated the index for both sets of samples and find that the CIA based on the CsCl treated samples has higher values than the non-treated aliquots (Fig. 3D). CEC of samples has a range from 42 to 49 over the core depth covered in this study (Fig. 3E). Measurements of CEC and CIA have an inverse relationship ($R^2=0.47$)(Fig. 6). High measurements of CIA indicate high chemical weathering in rocks, given that aluminum remains in the weathering residue. Low CEC indicates a breakdown of primary minerals to secondary clay minerals as a consequence of weathering. Here, a lower CIA, suggesting lower chemical weathering extent, correlates negatively with higher measurements of CEC, suggesting lower degrees of secondary mineral formation.

5. Discussion

542

5.1 The effects of adsorbed cation removal and CsCl wash on clay geochemistry

544

5.1.1 Major and trace elements abundant in seawater removed by exchange wash

546

Our geochemical results demonstrate that Na concentrations are most affected by the CsCl rinse, reduced by 75% (Supplementary Table, Fig. 2A). This suggests that much of the material bound to the clay surface is Na^+ ions, far and away the most abundant ion in seawater. Cs^+ replaces Na^+, bound to the surface of the clay, during the washing procedure due to the powerful hydration sphere of the Cs^+ and the high concentration of ions available for the exchange in the 0.1 molar solution. Also affected are Ca, Mg, and K concentrations, the 3rd, 5th, and 6th most abundant elements dissolved in seawater.

This change in our perception of major element chemistry has consequences. The CIA of marine sediment, dependent on concentrations of major elements, is commonly used as both a tracer and to appraise changes in weathering on the landscape (Garzanti et al., 2014)]. Here, our CIA measurements are higher using the Cs^+ treated value compared to the non-treated aliquots (Fig. 3D). This pattern results from the 75% reduction in the Na values in the Cs^+ washed sediment. We argue that this CIA measurement after the exchange wash provides a more realistic terrestrial signal, appraising the concentrations of only the structural components of the clay. The composition and rate of authigenic cation binding to clay minerals could depend on salinity and pH of seawater, transport pathways, and depositional environment, factors that could change on varying timescales.

We find reduced concentrations of strontium and neodymium in all samples that have undergone the Cs^+ cation exchange wash. Sr concentration in seawater is relatively high for a trace element, at ~10 ppm (Angino et al., 1966). The source of strontium is rocks of the continental crust delivered to the ocean in sediments, but it is highly soluble like its alkaline earth relative calcium and has a long residence time in seawater of ~5 Myr [*Palmer and Elderfield*, 1985]. Nd is also sourced from the continental crust and sediments but has a much lower concentration (~0.1-0.3 ppb) and much shorter residence time (200-1000 years)(Goldstein and O'Nions, 1981; Tachikawa et al., 2003; van de Flierdt et al., 2016). We attribute the loss of these elements to the fact that seawater derived Sr and Nd that has been adsorbed on the clay's surface in the marine environment are exchanged away with the CsCl solution. The isotopic composition of this material displaced by Cs^+ ions may have the potential to bias our measurements if not accounted for or removed.

579

How and when are cations usually adsorbed onto the surface of the clay? Studies have shown that diagenesis of clay minerals may occur when they are transferred from freshwater to seawater via the river system. The mechanism involves reactions of the cations and anions in seawater with the minerals through exchange, whereby a rearrangement of the cations in the exchange positions takes place (Carroll and Starkey, 2013).

586

Accounting for the conservation of charge in our data was a challenge: 4 of the 8 samples failed to achieve balance from the exchange. 3 samples appeared to collect more Cs than equivalents of soluble major elements were displaced, a positive balance. We offer a likely explanation for this set: organic matter in the finest fraction may have absorbed additional Cs in a way that we did not account for. This yields an important takeaway: given the very high cation exchange capacity of organic matter, it could contribute to CEC significantly even with relatively low concentrations of organic matter in bulk sediment. Therefore, we advise a step to oxidize organic matter to be introduced before the cation exchange wash.

Other problems contributing to the imbalance may be rooted in 1) analytical uncertainty in major elements and/or Cs leading to an accumulated error larger than we thought. Ca concentrations were difficult to measure because of its low concentration but Ca did not contribute to the charge balance enough to explain the observed imbalance. 2) the partial dissolution of clay minerals during the cation wash, limiting the ability of the clay to hold charge, contributing to a negative balance. This is also highly unlikely given the reagent was a low concentration (0.1 N) salt solution, with a pH of 4.5. More work would be needed to fully evaluate the charge balance.

5.1.2 Effects on radiogenic isotopes

The cation exchange wash may improve the fidelity of the radiogenic isotope proxies. Our logic is that if the different provenance proxies correlate more strongly with one another after the wash, that regression line must be pointing more accurately towards the isotopic composition of the source, or mixing sources.

The present-day seawater $^{87}Sr/^{86}Sr$ is 0.70918 (Henderson et al., 1994). In this study, we find $^{87}Sr/^{86}Sr$ between 0.74 and 0.77 (Supplementary Table), which points to a continental detritus origin of the signal. Two out of six samples treated with the Cs^+ wash yield more radiogenic ratios than before the treatment (beyond the measurement error of 0.00001), which could be explained by the removal of seawater derived Sr from the clay surface, thus altering the ratio towards more radiogenic values (Fig. 3A). Conversely, the remaining samples show the opposite $^{87}Sr/^{86}Sr$ trend, which cannot be explained by the removal of seawater derived Sr. However, in all cases, the removal of adsorbed Sr, whatever its isotopic composition, reveals $^{87}Sr/^{86}Sr$ values that correlate better with other isotopic measurements on the sample, as the CsCl wash improved correlations of Sr isotopes with other source-based proxies (εNd and $^{40}K/^{40}Ar$ age)(Fig. 4). Because of these improvements, the application of the cation wash is recommended for provenance studies employing Sr isotopes on clay minerals. While the observed magnitude of change on $^{87}Sr/^{86}Sr$ ratios from the CsCl washed aliquots is large (0.0025-0.08), and the correlations with the other isotopes are better, the overall trends in the correlations are the same, indicating that the general provenance interpretations of studies lacking a cation exchange wash are nevertheless valid.

All Cs^+-treated samples yield less radiogenic εNd values compared to their counterparts of 0.2–0.7 εNd units. The offsets are beyond the analytical uncertainty

of the measurement (error (2SD): 0.2 εNd units for the set of 16 samples), (Supplementary Table 1). Neodymium isotope ratios at ~500 m depth near our core site 1478 are ~ -12 (Jones, 2010). Exchanging away seawater authigenic Nd from the clay's surface would shift εNd values towards less radiogenic values as seen in our results. This would suggest that by applying a Cs$^+$ treatment the final εNd represents a purer detrital sediment signal overall. The removal of reabsorbed Nd from authigenic phases in seawater and the improved detrital signal of the sediment is also confirmed by the correlations (Fig. 4). All sample values become systematically less radiogenic however, the magnitude of this shift is small compared to potential shifts caused by a change in provenance.

For the five measured Pb isotope ratios, we cannot find any systematic offset, which makes it difficult to directly infer whether the wash leads to a more robust detrital signal. It could, however, also be governed by the fact that Pb, due to its low solubility, does not travel very far in seawater, possibly resulting in fairly similar compositions between authigenic and terrigenous phases.

Comparing the average εNd and $^{87}Sr/^{86}Sr$ values from our data set to the published values from the Limpopo catchment area indicates a good match within the reported range by Garzanti et al. (2014), which confirms the Limpopo system source of this detrital fraction. Minor deviations might be related to different grain size fractions measured in both studies and the applied sediment leaching techniques. The washed population with slightly less radiogenic average εNd values would indicate an even better match with the terrestrial dataset compared to the unwashed ones. We avoid making an attempt to interpret changes in sources through time based on our very limited dataset: only 8 samples spaced over ~10 m of core.

We find that the $^{40}K/^{40}Ar$ age of washed samples tend to be younger than the unwashed samples. We suggest this is the result of grain size and density effect in the process of creating the small clods (sample weights are 0.1-0.5 mg for the $^{40}Ar*$ measurements). Unwashed clods appear thin, glossy, and have a dark color. Replicate analyses on these clods consistently yield higher standard deviations than in the washed aliquot. Additionally, it appears older ages could result from a tendency to sample the densest parts of the clod, near the center of the microcentrifuge tube. In the washed clods, it does not appear to matter which part is sampled for analyses. Among clay minerals, illite is the only significant K-bearing one. It is also denser (2.6-2.9 specific gravity) than minerals from the smectite group (montmorillonite = 1.7-2.0). Thus, in dried unwashed samples, the center of the clod might contain the oldest, densest clay minerals. In dried, Cs washed aliquots however, selecting different parts of the sample yielded the same $^{40}Ar*$ concentrations. Clay flocculates more readily in the Cs ion rich solution of the washed samples, causing them to settle more quickly and uniformly, and thus reducing the sorting effect and providing a more homogenized $^{40}Ar*$ measurement. Experimentation confirmed this in the unwashed aliquot, and this effect can be mostly corrected for by weighing and measuring the entire sample clod.

We conclude our discussion by restating our inference that the exchange wash has the effect of improving correlations between isotopic measurements on a set of samples because the removed adsorbed cations obscure the true, terrigenous signal

679 endemic to the clays of the sample. Variations in local dissolved seawater cations,
680 the aqueous geochemistry of the river catchment, changes in salinity or pH of
681 seawater, transport processes and duration, and landscape storage are among the
682 list of many potential factors that could affect the chemical composition of cations
683 bound to clay minerals. These might have the effect of biasing that terrestrial signal.

684

685 **5.2 Potential additional indicators of environmental information: The**
686 **application of the Chemical Index of Alteration (CIA) and Cation exchange**
687 **capacity (CEC) of the clay fractions**

688 Positively-charged ions are adsorbed to soil surfaces by the electrostatic interaction
689 between their positive charge and the negative charge of the surface (Schaetzl and
690 Thompson, 2015). Exchangeable cations thus form part of the diffuse layer above
691 the charged surface. These cations can easily be displaced from the surface by other
692 cations from a surrounding solution, as the binding is relatively weak. Cation-
693 exchange capacity is measured by displacing all the bound cations with a
694 concentrated solution of another cation, and then measuring either the displaced
695 cations in solution or the amount of added cation that is retained on the solid (Bache,
696 1976). In this study, we used a CsCl solution because Cs^+ is a trace element in the
697 natural solids and thus its concentration in the washed sample is a potential
698 measure of the CEC.

699

700 CIA and CEC have an inverse relationship and are moderately correlated (Fig. 6).
701 However, a poor correlation might be expected because the proxies are not sensitive
702 to exactly the same processes. CIA was designed to quantify degree of bedrock
703 weathering, and thus would be sensitive to sediment source sorting processes. A
704 study from Changjiang River basin, China has questioned whether the CIA reflects
705 silicate weathering, and concluded that it probably indicates the integrated
706 weathering history in the river basin, and thus, cannot be used as a reliable proxy of
707 instantaneous chemical weathering (Shao and Yang, 2012). Furthermore, the
708 hydrodynamic sorting also influences the CIA values. On the other hand, the CEC
709 may be sensitive to the climate of the clay minerals' formation, and the residence
710 time of the sediment on the landscape. In one endmember scenario, extremely high
711 rates of physical weathering and erosion could result in the deposition of primary
712 minerals with low CEC, such as the glacial flour in Owens Lake (Bischoff et al., 1997).
713 In another endmember scenario, low rates of erosion coupled with high soil flushing
714 could produce laterite soils, rich in Fe and Al oxides, which would also have
715 extremely low CEC.

716 This study shows that a CsCl exchange wash can be applied to marine sediments
717 (sensitive to terrestrial input from land) to derive the cation exchange capacity in
718 clay minerals. The CEC measurement gave a qualitative prediction of the clay
719 mineralogy of the sample, as the proportion of kaolinite to smectite appeared to
720 control CEC. Because clay mineralogy relates to terrestrial weathering processes,
721 there is a potential for CEC to indicate climate conditions and chemical weathering
722 extent. In our data, the CEC is inversely proportional to the weathering index CIA,
723 with more aluminous, high CIA samples correlating with low CEC samples that have
724 more simple clay minerals.

6. Conclusions

We present a recommended sediment leach protocol for an improved terrigenous signature extraction from marine sediments that includes a cation exchange wash. We find that ions having higher concentrations in seawater are predominantly displaced by the cation exchange wash, and conclude that the derived geochemical data represents a more accurate terrestrial signal. Therefore, this procedure is favourable for major and trace elements and leads to Nd and Sr isotope ratios that are more truly representative of the terrestrial detritus. The observed magnitude of change in the Sr and Nd isotopes between washed and non-washed aliquots is large. Nevertheless, whether the Cs^+-treatment was used or not, the overall downcore trends and correlations between isotopes are similar, and hence whether or not it is applied, general climate reconstruction conclusions are likely to be similar.

Due to flocculation and rapid settling of clay minerals in Cs-washed samples, it is evident that a dried Cs-washed aliquot is more homogenous, and that $^{40}K/^{40}Ar$ age measured on it will be more reproducible and reflect the bulk age of the sediment.

For the accurate determination for the CEC of the clay fraction of marine sediment, we recommend adding to the procedure a step that oxidizes organic matter. This may be important, even if the concentration of organic matter in the sediment is low.

Because of the relationship between cation exchange capacity, clay mineralogy, soil flushing, and ultimately annual precipitation and climate conditions, CEC could, with further calibration efforts, be useful as a terrestrial chemical weathering proxy. However, CEC's potential in this capacity is difficult to tell due to the limited range of CEC (42-50 meq/100g) in this study. A detailed survey of CEC of clay minerals in different depositional and climate settings would be necessary to relate the CEC of the clay mineral fraction to chemical weathering regimes.

Author contributions: M.H.S and C.L raised the funding for this pilot study. S.H. and S.G. contributed financially to the analysis cost and hosted M.H.S. at LDEO where analyses were performed. S.H., M.H.S., and S.G. designed the initial idea for this pilot study. M.H.S. conducted much of the laboratory work for the sediment preparations, dissolution, and column chemistry. S.H. and D.B. conducted the major/trace element analysis for this study. D.B helped with K/Ar age analysis, designed the K/Ar age settling study. X.H. performed the clay mineralogy analyses. M.Y.C. supervised M.H.S. during laboratory work and conducted together with M.H.S. the isotope measurements. T.L. analyzed samples for K/Ar ages. M.J. and A.H. helped with testing protocols for the Cs-wash step and its effect on K/Ar ages. M.H.S and D.B. structured the outline of the paper and wrote the manuscript. All authors read and contributed to the final manuscript.

Appendix A. Supplementary data

Supplementary data associated with this article can be found in the online version.

References

Abouchami , W., Galer, S.J.G., 1998. The provinciality of Pb isotopes in Pacific Fe-Mn deposits. Mineralogical Magazine, 62A (1-2).

Allègre, C.J., Dupré, B., Négrel, P., Gaillardet, J., 1996. Sr-Nd-Pb isotope systematics in Amazon and Congo River systems: constraints about erosion processes. Chemical Geology, 131(1): 93-112.

Angino, E.E., Billings, G.K., Andersen, N., 1966. Observed variations in the strontium concentration of sea water. Chemical Geology, 1: 145-153.

Biscaye, P.E., 1965. Mineralogy and Sedimentation of Recent Deep-Sea Clay in the Atlantic Ocean and Adjacent Seas and Oceans. GSA Bulletin, 76(7): 803-832.

Bischoff, J.L., Menking, K.M., Fitts, J.P., Fitzpatrick, J.A., 1997. Climatic Oscillations 10,000–155,000 yr B.P. at Owens Lake, California Reflected in Glacial Rock Flour Abundance and Lake Salinity in Core OL-92. Quaternary Research, 48(3): 313-325.

Carroll, D., Starkey, H.C., 2013. EFFECT OF SEA-WATER ON CLAY MINERALS1 A2 - INGERSON, EARL, Clays and Clay Minerals. Pergamon, pp. 80-101.

Eglington, B.M., Armstrong, R.A., 2004. The Kaapvaal Craton and adjacent orogens, southern Africa: a geochronological database and overview of the geological development of the craton. South African Journal of Geology, 107(1-2): 13-32.

Esquevin, J., 1969. Influence de la composition chimique des illites sur leur cristallinité. Bulletin du Centre de Recherches de Pau-SNPA 3: 147–153

Franzese, A.M., Hemming, S.R., Goldstein, S.L., 2009. Use of strontium isotopes in detrital sediments to constrain the glacial position of the Agulhas Retroflection. Paleoceanography, 24(2): PA2217.

Franzese, A.M., Hemming, S.R., Goldstein, S.L., Anderson, R.F., 2006. Reduced Agulhas Leakage during the Last Glacial Maximum inferred from an integrated provenance and flux study. Earth and Planetary Science Letters, 250(1–2): 72-88.

Garzanti, E., Padoan, M., Setti, M., López-Galindo, A., Villa, I.M., 2014. Provenance versus weathering control on the composition of tropical river mud (southern Africa). Chemical Geology, 366: 61-74.

Goldstein, S.L., O'Nions, R.K., 1981. Nd and Sr isotopic relationships in pelagic clays and ferromanganese deposits. Nature, 292(5821): 324-327.

Goldstein, S.L., O'Nions, R.K., Hamilton, P.J., 1984. A Sm-Nd isotopic study of atmospheric dusts and particulates from major river systems. Earth and Planetary Science Letters, 70(2): 221-236.

Gombiner, J.H., Hemming, S.R., Hendy, I.L., Bryce, J.G., Blichert-Toft, J., 2016. Isotopic and elemental evidence for Scabland Flood sediments offshore Vancouver Island. Quaternary Science Reviews, 139: 129-137.

819 Gutjahr, M. et al., 2007. Reliable extraction of a deepwater trace metal isotope signal from
820   Fe–Mn oxyhydroxide coatings of marine sediments. Chemical Geology, 242(3):
821   351-370.
822 Hahn, A. et al., 2016. Holocene paleo-climatic record from the South African Namaqualand
823   mudbelt: A source to sink approach. Quaternary International, 404, Part B: 121-
824   135.
825 Hall, I., Hemming, S., LeVay, L. , Barker, S. , Berke, M. , Brentegani, L. , Caley, T. , Cartagena-
826   Sierra, A. , Charles, C. , Coenen, J. , Crespin, J. , Franzese, A. , Gruetzner, J. , Han, X. ,
827   Hines, S. , Jimenez Espejo, F. , Just, J. , Koutsodendris, A. , Kubota,, K. , L., N. , Norris,
828   R. , Periera dos Santos, T. , Robinson, R. , Rolinson, J. , Simon, M. , Tangunan, D. , van
829   der Lubbe, J. , Yamane, M. and Zhang, H. , 2017. Expedition 361 summary.
830   Proceedings of the International Ocean Discovery Program 361.
831 Haughton, P.D.W., Todd, S.P., Morton, A.C., 1991. Sedimentary provenance studies.
832   Geological Society, London, Special Publications, 57(1): 1-11.
833 Hemming, S.R. et al., 2002. 40Ar/39Ar ages and 40Ar* concentrations of fine-grained
834   sediment fractions from North Atlantic Heinrich layers. Chemical Geology, 182(2):
835   583-603.
836 Henderson, G.M., Martel, D.J., O'Nions, R.K., Shackleton, N.J., 1994. Evolution of seawater
837   87Sr86Sr over the last 400 ka: the absence of glacial/interglacial cycles. Earth and
838   Planetary Science Letters, 128(3): 643-651.
839 Imai, N., Terashima, S., Itoh, S., Ando, A., 1996. Compilation of analytical data on nine GSJ
840   Geochemical reference samples "Sedimentary rock series". Geostandards
841   Newsletter, 20(2): 165-216.
842 Jacobsen, S.B., Wasserburg, G.J., 1980. Sm-Nd isotopic evolution of chondrites. Earth and
843   Planetary Science Letters, 50(1): 139-155.
844 Jelsma, H.A., Dirks, P.H.G.M., 2002. Neoarchaean tectonic evolution of the Zimbabwe
845   Craton. Geological Society, London, Special Publications, 199(1): 183-211.
846 Jiménez-Espinosa, R., Vázquez, M., Jiménez-Millán, J., 2007. Differential weathering of
847   granitic stocks and landscape effects in a Mediterranean climate, Southern Iberian
848   Massif (Spain). CATENA, 70(2): 243-252.
849 Jones, K., 2010. An evaluation of radiogenic isotopes as tracers of ocean circulation and
850   sediment transport: Ocean modeling, seawater analysis, and sediment studies,
851   Columbia University, New York. US.
852 Jung, S.J.A., Davies, G.R., Ganssen, G.M., Kroon, D., 2004. Stepwise Holocene aridification in
853   NE Africa deduced from dust-borne radiogenic isotope records. Earth and
854   Planetary Science Letters, 221(1–4): 27-37.
855 Kreissig, K., F Nägler, T., Kramers, J., van Reenen, D., Smit, C.A., 2000. An isotopic and
856   geochemical study of the northern Kaapvaal Craton and the Southern Marginal
857   Zone of the Limpopo Belt: Are they juxtaposed terranes?, 50, 1-25 pp.
858 Lamont, T., Roberts, M.J., Barlow, R.G., and van den Berg, M.A., 2010. Circulation patterns in
859   the Delagoa Bight, Mozambique, and the influence of deep ocean eddies. African
860   Journal of Marine Science, 32(3): 553-562.
861 Lutjeharms, J.R.E., 2006. Three decades of research on the greater Agulhas Current. Ocean
862   Sci. Discuss., 3(4): 939-995.
863 Milliman, J.D., Meade, R.H., 1983. World-Wide Delivery of River Sediment to the Oceans.
864   The Journal of Geology, 91(1): 1-21.
865 Morad, S., Ketzer, J.M., De Ros, L.F., 2000. Spatial and temporal distribution of diagenetic
866   alterations in siliciclastic rocks: implications for mass transfer in sedimentary
867   basins. Sedimentology, 47(s1): 95-120.
868 Nesbitt, H.W., Young, G.M., 1982a. Early Proterozoic climates and plate motions inferred
869   from major element chemistry of lutites. Nature, 299: 715.

870 Nesbitt, H.W., Young, G.M., 1982b. Early Proterozoic climates and plate motions inferred
871   from major element chemistry of lutites. Nature, 299(5885): 715-717.
872 Odin, G.S., 1976. La glauconite GL-O, étalon inter-laboratoires pourl'analyse
873   radiochronométrique. Analusis, 4: 287-291.
874 Reason, C.J.C., Jury, M.R., 1990. On the generation and propagation of the southern African
875   coastal low. Quarterly Journal of the Royal Meteorological Society, 116(495):
876   1133-1151.
877 Reason, C.J.C., Landman, W., Tennant, W., 2006. Seasonal to Decadal Prediction of Southern
878   African Climate and Its Links with Variability of the Atlantic Ocean. Bulletin of the
879   American Meteorological Society, 87(7): 941-955.
880 Rutberg, R.L., Goldstein, S.L., Hemming, S.R., Anderson, R.F., 2005. Sr isotope evidence for
881   sources of terrigenous sediment in the southeast Atlantic Ocean: Is there increased
882   available Fe for enhanced glacial productivity? Paleoceanography, 20(1): PA1018.
883 Schüürman, J., Hahn, A., Zabel, M., 2019. In search of sediment deposits from the Limpopo
884   (Delagoa Bight, southern Africa): Deciphering the catchment provenance of coastal
885   sediments. Sedimentary Geology, 380: 94-104.
886 Shao, J., Yang, S., 2012. Does chemical index of alteration (CIA) reflect silicate weathering
887   and monsoonal climate in the Changjiang River basin? Chinese Science Bulletin,
888   57(10): 1178-1187.
889 Tachikawa, K., Athias, V., Jeandel, C., 2003. Neodymium budget in the modern ocean and
890   paleo-oceanographic implications. Journal of Geophysical Research: Oceans,
891   108(C8).
892 Tanaka, T. et al., 2000. JNdi-1: a neodymium isotopic reference in consistency with LaJolla
893   neodymium. Chemical Geology, 168(3): 279-281.
894 Tessier, A., Campbell, P.G.C., Bisson, M., 1979. Sequential extraction procedure for the
895   speciation of particulate trace metals. Analytical Chemistry, 51(7): 844-851.
896 Tyson, P.D., Preston-Whyte, R.A., 2000. The Weather and Climate of Southern Africa.
897   Oxford University Press: Cape Town.
898 van de Flierdt, T. et al., 2016. Neodymium in the oceans: a global database, a regional
899   comparison and implications for palaeoceanographic research. Philosophical
900   Transactions of the Royal Society A: Mathematical, Physical and Engineering
901   Sciences, 374(2081): 20150293.
902 van der Lubbe, H.J.L., Frank, M., Tjallingii, R., Schneider, R.R., 2016. Neodymium isotope
903   constraints on provenance, dispersal, and climate-driven supply of Zambezi
904   sediments along the Mozambique Margin during the past ~45,000 years.
905   Geochemistry, Geophysics, Geosystems, 17(1): 181-198.
906 Weis, D. et al., 2006. High-precision isotopic characterization of USGS reference materials
907   by TIMS and MC-ICP-MS. Geochemistry, Geophysics, Geosystems, 7(8): n/a-n/a.
908 Zabel, M., Bickert, T., Dittert, L., Haese, R.R., 1999. Significance of the sedimentary Al:Ti
909   ratio as an indicator for variations in the circulation patterns of the equatorial
910   North Atlantic. Paleoceanography, 14(6): 789-799.
911

912 **Figure captions**

913

914 **Figure 1:** Location map of IODP Site U1478 with main surface currents (arrows) in the
915 southwest Indian Ocean and atmospheric circulation over southern Africa during austral
916 summer (December, January, February) with approximate position of the Intertropical
917 Convergence Zone (ITCZ) and Congo Air Boundary (CAB) (dashed lines; adapted from
918 Reason et al. (2006). AC = Agulhas Current, SEC = South Equatorial Current, SEMC = South
919 East Madagascar Current, NEMC = North East Madagascar Current, EACC = East Africa

920 Coastal Current. Purple shading = Zambezi Catchment, green shading = Limpopo Catchment,
921 gray double-headed arrows = main pathways of moisture supply to the African continent
922 from the northwest Atlantic (through Congo) and the northwest and southwest Indian
923 Ocean (taken from Hall et al. (2017)).

924 **Figure 2: A)** The magnitude of the reduction in the concentration of an element as a result
925 of the cation exchange wash, expressed as a percent of the concentration of the unwashed
926 group. Sample IDs are listed in table 2-4 for reference. The elements bound to the clay
927 surface in the highest relative concentrations are Na, Ca, Mn, Ba, and Sr. **B)** The equivalents
928 of cation displaced must equal the equivalents of Cs measured to conserve charge. The
929 residual between the concentrations of the major elements in the test group (washed) and
930 the control group (unwashed) was calculated, then converted to equivalents. Here, we
931 visualize the summation of these charges, element-wise, for each sample. The average of all
932 samples is plotted behind as a thick black line, with a ±1σ standard deviation envelope
933 surrounding it (light grey). Ideally, the cumulative sum of these losses should equal the
934 equivalents of Cs. The more equivalents of Na, Mg, K, and Ca a sample lost, the higher its Cs
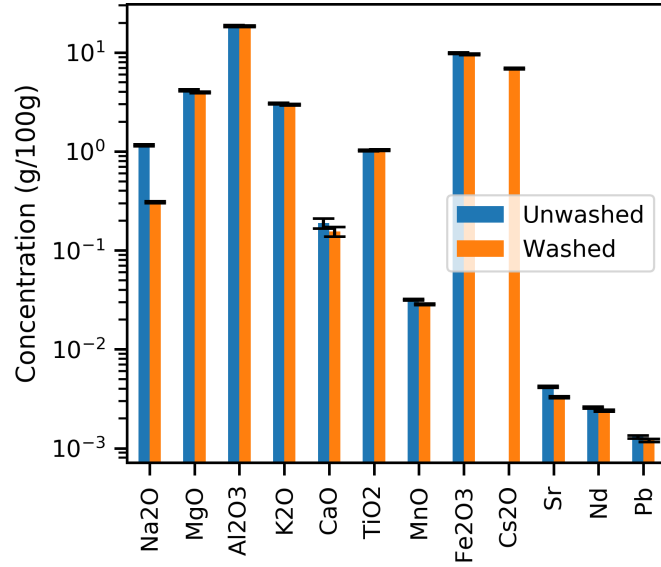935 concentration and cation exchange capacity should be.

936 **Figure 3:** Overview of relative compositions of CsCl treated and non-treated samples
937 against core depth in m**.** Red displays the CsCl treated aliquot for each sample. A:
938 Comparison for $^{87}Sr/^{86}Sr$, average (n=16) $^{87}Sr/^{86}Sr$ 2 SE measurement error: 0.000012; B:
939 εNd; average (n=16) 2 SE measurement error: 0.07;C: ^{40}Ar model age in Ma calculated using
940 the 2% K, error is the ± 1s (Ma); D: Chemical Index of Alteration (CIA, (Nesbitt and Young,
941 1982a)); E: Cation exchange capacity (CEC,); F: $^{206}Pb/^{204}Pb$, average (n=16) 2 SE
942 measurement error 0.0004 G: $^{207}Pb/^{204}Pb$, average (n=16) 2 SE measurement error:
943 0.00036 H: $^{208}Pb/^{204}Pb$, average (n=16) 2 SE measurement error: 0.001044; I: $^{208}Pb/^{206}Pb$,
944 average (n=16) 2 SE measurement error: 0.00023; J: $^{207}Pb/^{206}Pb$, average (n=16) 2 SE
945 measurement error: 0.00010.

946 **Figure 4: (Left set of panels)** Left panels show correlations between the control group
947 (non treated aliquots) and right panels display correlations between test groups (CsCl -
948 washed). R^2 correlation coefficients displayed at the bottom of each plot **A)** Correlations of
949 εNd and $^{87}Sr/^{86}Sr$ and (Ma) **B)** Correlations of ^{40}Ar model age (Ma) and $^{87}Sr/^{86}Sr$ **C)**
950 Correlations $^{40}K/^{40}Ar$ (Ma) and $^{87}Sr/^{86}Sr$. **D)** Correlations of $^{40}K/^{40}Ar$ (Ma) and ^{40}Ar model
951 age (Ma)**. E)** Correlations of εNd and ^{40}Ar model age (Ma). **F)** Correlations of εNd and
952 $^{40}K/^{40}Ar$ (Ma). **(Right)** Correlation matrices were generated to evaluate the effect of CsCl
953 wash holistically. Warmer colors represent higher degrees of correlation. **G)** R^2 values
954 without the CsCl wash. **H)** R^2 values of clays washed with CsCl. **I)** The effects of the
955 procedure are better visualized by subtracting the washed (H) and unwashed (G) matrices,
956 visualizing the difference before and after the procedure.   Correlations of $^{87}Sr/^{86}Sr$ to
957 $^{40}K/^{40}Ar$ and εNd are notably improved by the CsCl wash, depicted with warmer colors.

958 **Figure 5**: Clay mineral content down core of the 8 test samples from IODP Site U1478
959 without CsCl treatment.

960

Bathymetry [m]
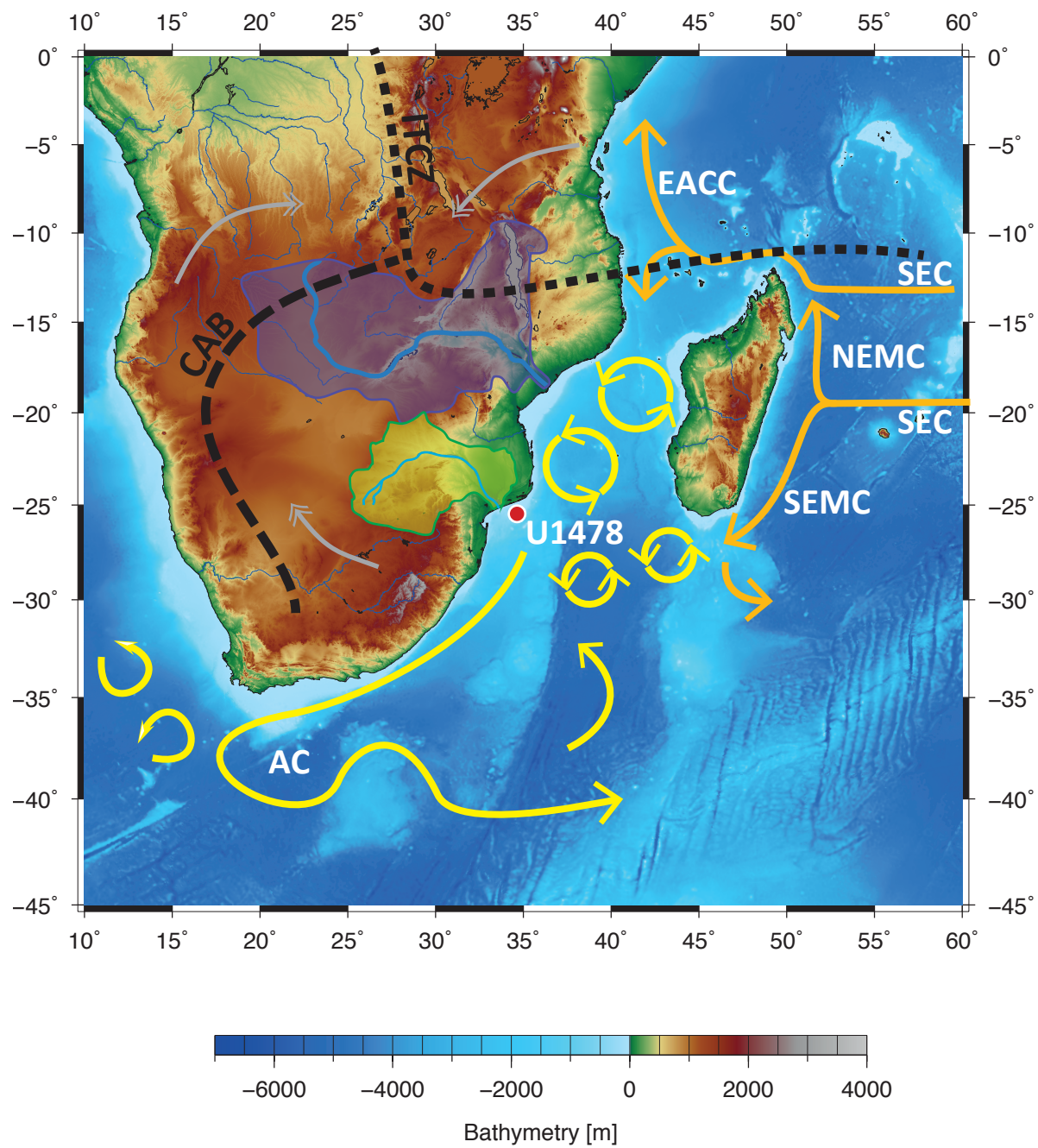
Mean Major Element Weight Corrected Concentrations,
Unwashed and Washed, n=8

Charge Balance Assessment